

Supplement of The Cryosphere, 14, 1595–1609, 2020
<https://doi.org/10.5194/tc-14-1595-2020-supplement>
© Author(s) 2020. This work is distributed under
the Creative Commons Attribution 4.0 License.



Supplement of

Combining TerraSAR-X and time-lapse photography for seasonal sea ice monitoring: the case of Deception Bay, Nunavik

Sophie Dufour-Beausé

Correspondence to: Sophie Dufour-Beauséjour (sophie.dufour-beausejour@ete.inrs.ca)

The copyright of individual parts of the supplement might differ from the CC BY 4.0 License.

Change detection and linear regression on backscattering time-series

Here we present range estimations for seasonal features in Fig. S1, S2 and S3 (post-freeze-up and spring peak, beginning and end of monotone backscattering), as well as the linear regressions on the monotone winter backscattering in Fig. S4.

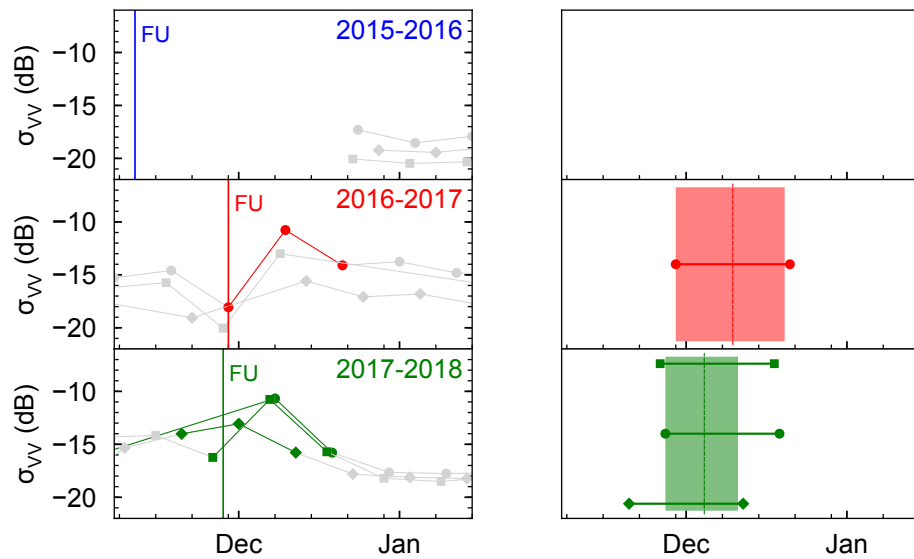


Figure S1: Post-freeze-up peak estimation. Left: TerraSAR-X median VV in orbits 13 (square), 21 (circle) and 89 (diamond). Markers used for peak estimation are in color, the rest of the series is in gray. For reference, freeze-up is identified with a vertical line. Right: Peak ranges reproduced from left. The range obtained from combining all orbits is color-shaded. Peak estimation is indicated with a dashed line. Data is color-coded for each year.

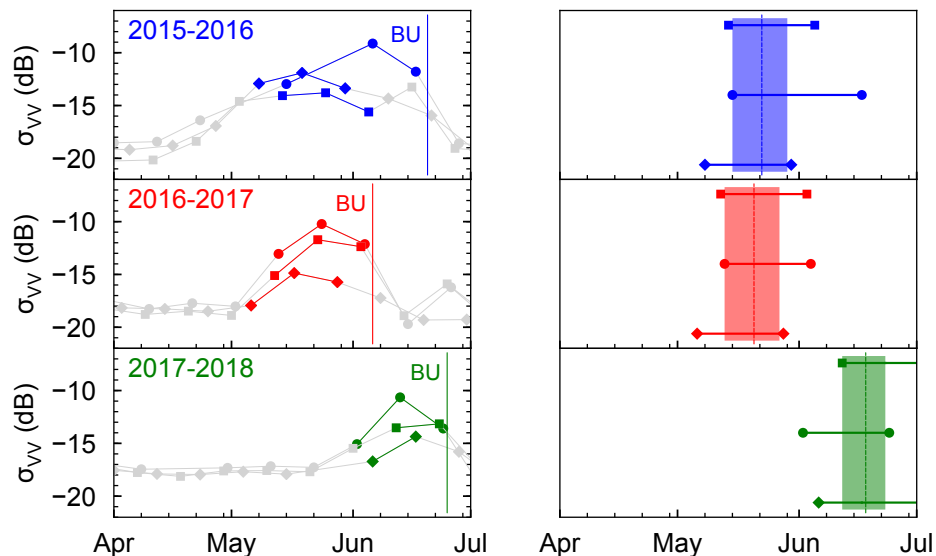


Figure S2: Spring peak estimation. Left: TerraSAR-X median VV in orbits 13 (square), 21 (circle) and 89 (diamond). Markers used for peak estimation are in color, the rest of the series is in gray. For reference, break up is identified with a vertical line. Right: Peak ranges reproduced from left. The range obtained from combining all orbits is color-shaded. Peak estimation is indicated with a dashed line. Data is color-coded for each year.

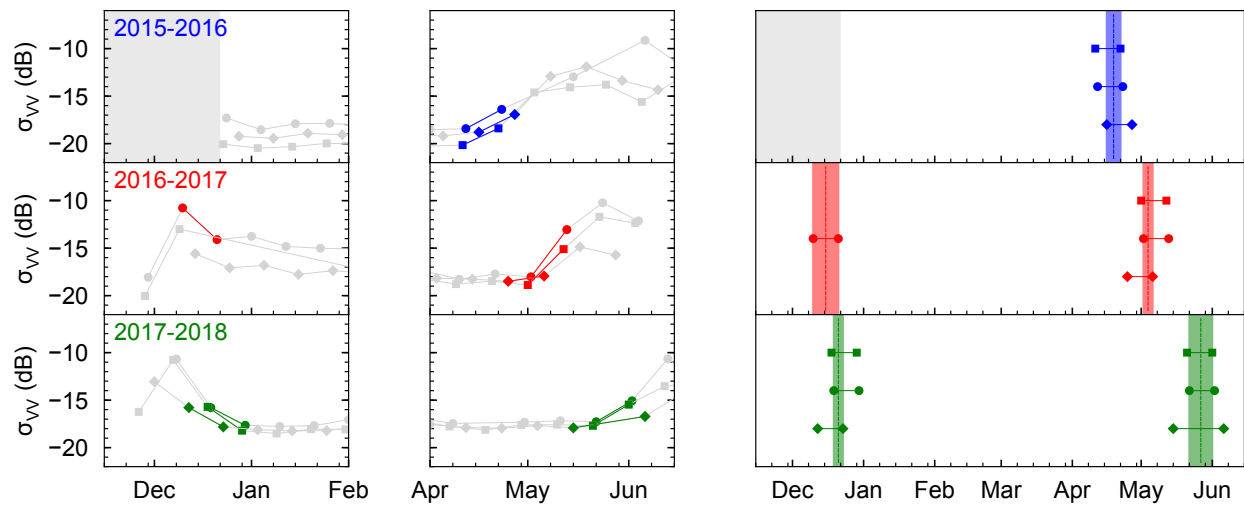


Figure S3: Monotone backscattering limits estimation. Left and center: TerraSAR-X median VV in orbits 13 (square), 21 (circle) and 89 (diamond). Markers used for limit estimation are in color, the rest of the series is in gray. Right: Limit ranges reproduced from left and center. The ranges obtained from combining all orbits are color-shaded. Limit estimation is indicated with a dashed line. Data is color-coded for each year.

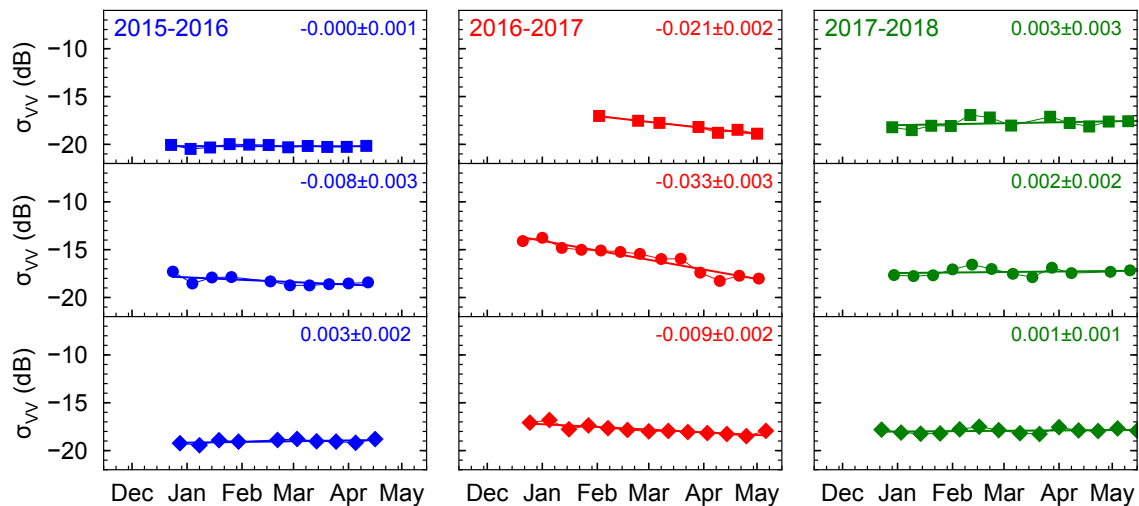


Figure S4: TerraSAR-X median VV backscattering during the monotone period. Observations are plotted for each orbit (orbit 13: squares, orbit 21: circles, orbit 89: diamonds) and color-coded for each year. The linear regression on the data is plotted as a solid line. Slope and standard error are indicated in the top right corner.

Newly formed ice on TerraSAR-X images

Here we present TerraSAR-X VV images featuring newly formed ice as identified from co-interpretation with time-lapse photography.

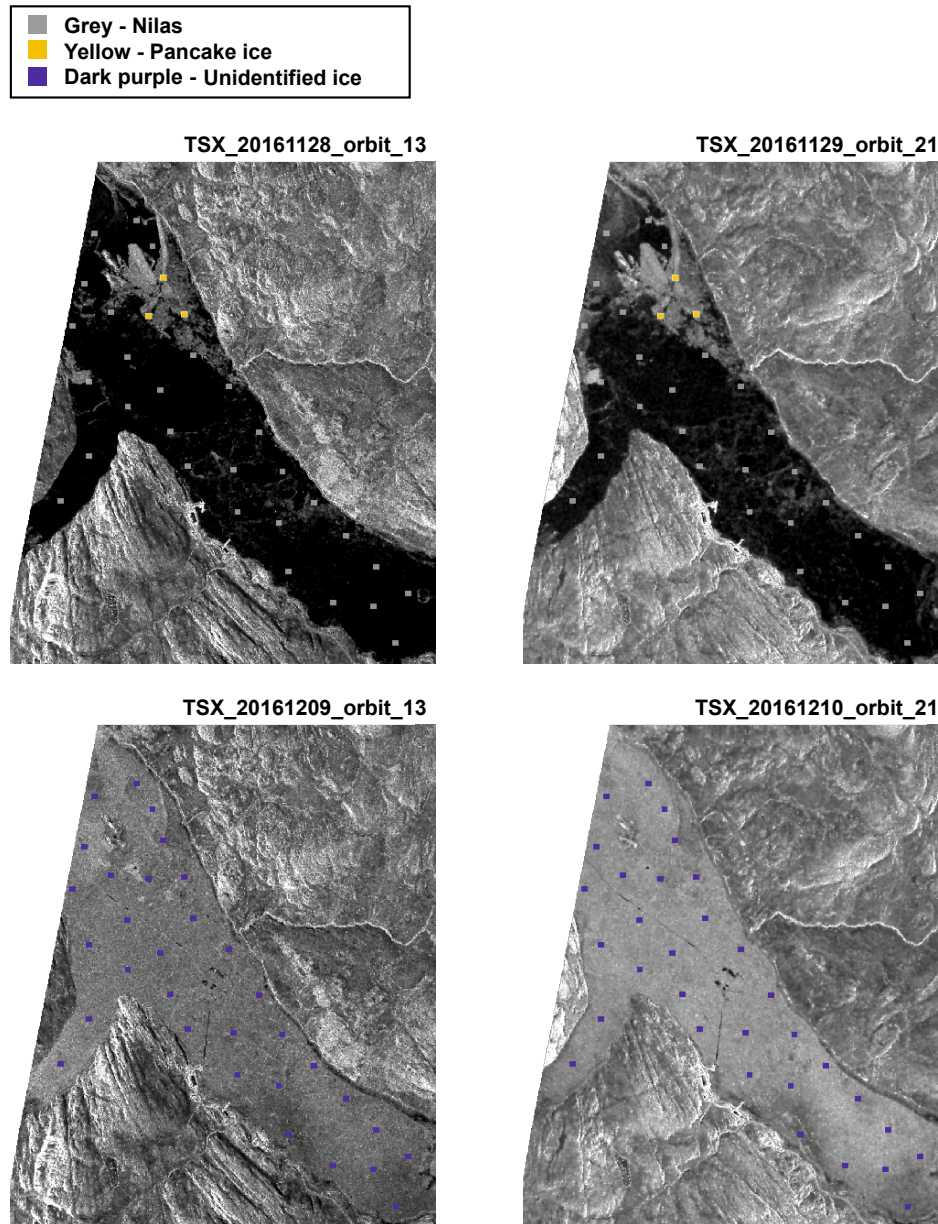
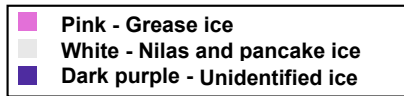
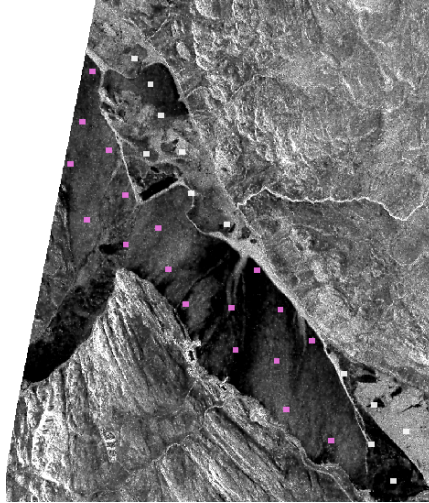


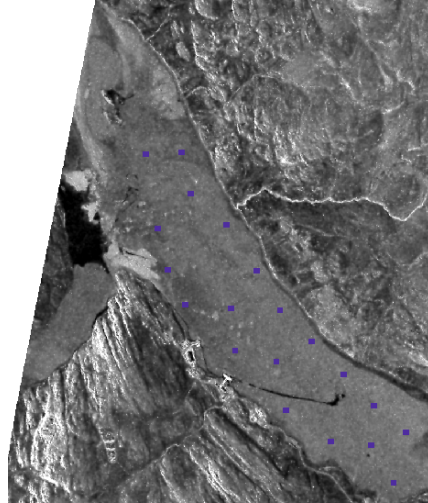
Figure S5: TerraSAR-X VV images of newly formed ice in 2016 (scaled from -19 to -5 dB) and AOIs used to compute statistics.



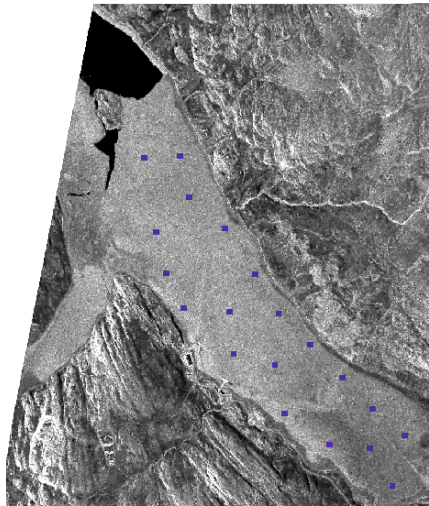
TSX_20171126_orbit_13



TSX_20171201_orbit_89



TSX_20171207_orbit_13



TSX_20171208_orbit_21

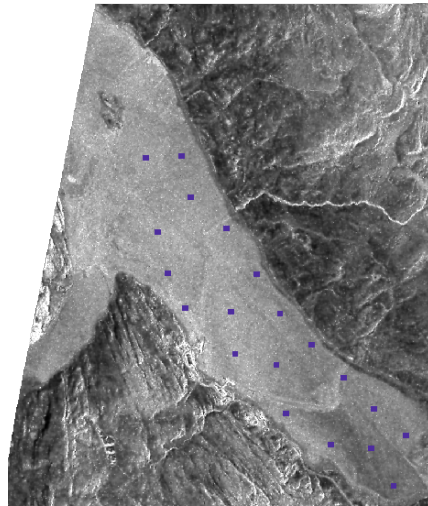


Figure S6: TerraSAR-X VV images of newly formed ice in 2017 (scaled from -19 to -5 dB) and AOIs used to compute statistics.

Air temperature in Deception Bay

In the absence of weather station in Deception Bay, two alternative sources were investigated for the air temperature: the nearest weather station located 50 km away at Salluit airport and camera measurements in Deception Bay.

Data acquisition and description

The closest weather station to Deception Bay is located in neighboring Salluit at the airport. Measurements at the station are taken hourly during the day and their daily mean is available online from Environment Canada. Salluit is a Nunavik coastal community located 50 km west of Deception Bay; the airport is located 2.8 km inland at an altitude of 226 m.

Two Reconyx PC800 Hyperfire Professional Semi Covert cameras were installed in Deception Bay as part of the CAIMAN research project. These cameras were installed near the study area, in front of Moosehead Island at an altitude of 22 m (series A) and on Black Point at an altitude of 33 m (series B), as shown on Fig. S7. They rely on 12 V batteries and solar panels for power and are mounted at 1.8 meters above the ground. They measure the temperature within the camera case and record this information in the photographs' metadata. Data is available hourly during the day between 7:00 and 18:00 local time; a daily mean is computed from this daytime data.

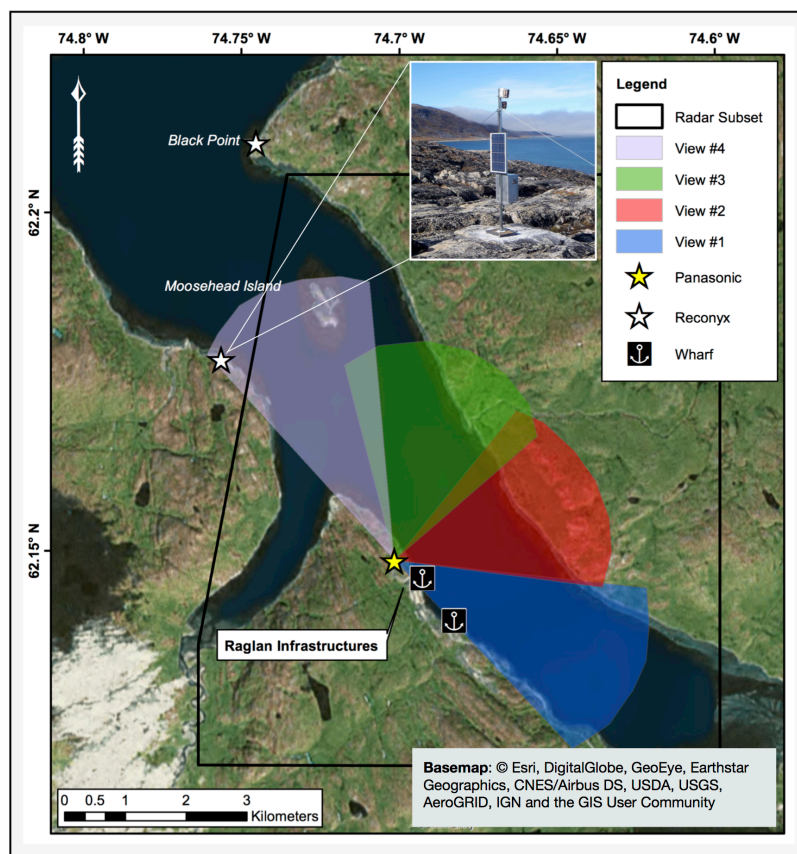


Figure S7: Map of time-lapse camera locations and Panasonic fields of view. Inset: Reconyx camera on the south-western shore in front of Moosehead Island (solar panel and battery also shown).

Temperature time-series were assembled from photograph metadata for two cameras: Moosehead Island (Series A) and Black Point (Series B). Series A was continuous over the study period except for a gap between 27 January and 18 September 2016. Series B extends from 11 September 2015 to 16 September 2016. The two series were compared for the overlapping period (11 September 2015 to 27 January 2016). The difference between series A and B was 0.4 °C on average, with a standard deviation of 0.7 °C. This was deemed sufficiently small to combine the two series with no transformation. Series B was used up to 16 September 2016 and series A from 18 September 2016. Since the Reconyx temperature sensor sometimes erroneously recorded a 0°C measurement in lieu of “not-a-number”, all 0 °C values were removed from the datasets.

Comparing camera and airport measurements

Figure S8 shows the camera and airport datasets from 2015 to 2018. The camera and airport measurements showed a Pearson coefficient of 0.98 and 0.99 for the three years of the study, which proves a strong correlation despite their different locations. The camera dataset however differs from the airport’s dataset with a root mean-squared-error (RMSE) of 3.9 to 4.3°C. In order to investigate this discrepancy, the daily difference between the two datasets is also plotted in Fig. S8. This difference is roughly flat from September to January, and then peaks in April-May.

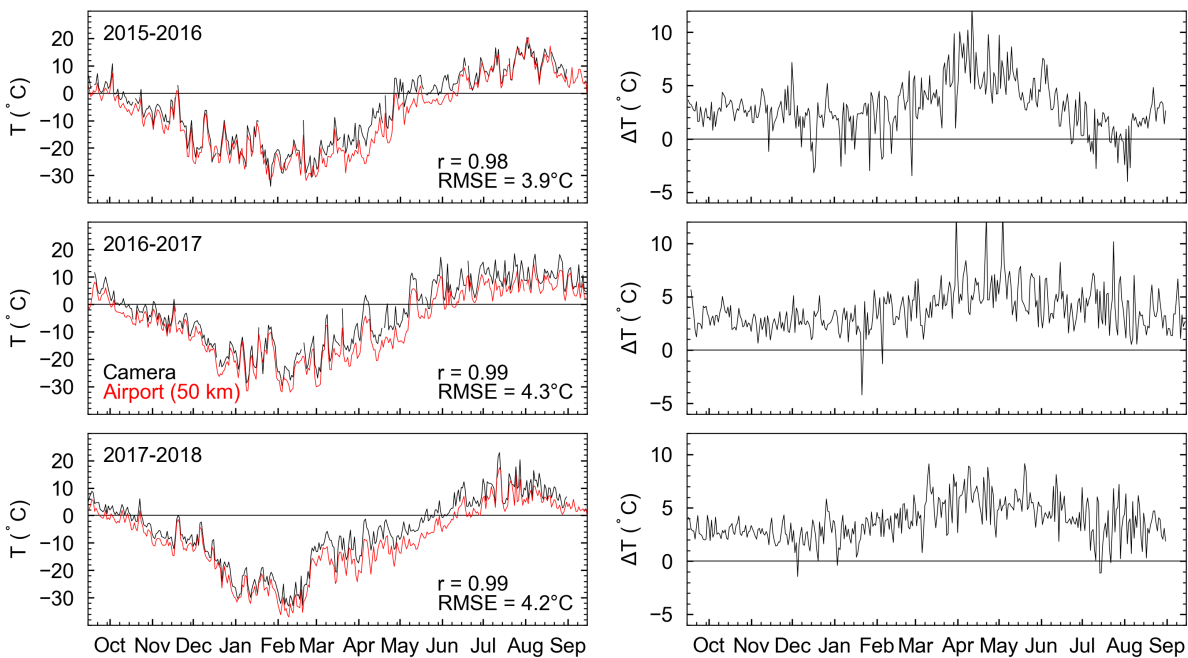


Figure S8: Left: Daily mean air temperature measured by the camera in Deception Bay (black) and at the Salluit airport (red). Right: Daily difference between the two datasets.

Several factors may cause differences between temperature measurements by the cameras in Deception Bay and at the Salluit airport. First, temperatures might actually be different between the two locations; the airport is located inland while the camera is located on the shore, the airport is roughly 200 m higher in terms of altitude, and it is located 50 km west of the cameras. Second, the camera measurement may suffer from measurement biases: for example, heating of the camera by the sun may increase the temperature around the sensor.

Mean air temperature at Salluit airport

Since the data measured 50 km away at Salluit airport is strongly correlated to the temperature measured with the cameras in Deception Bay, and because the camera data is shown to present a non-trivial seasonal bias, we chose to use the dataset from Salluit airport to compare the three years in terms of air temperature. Figure S9 shows the monthly mean air temperature at Salluit airport.

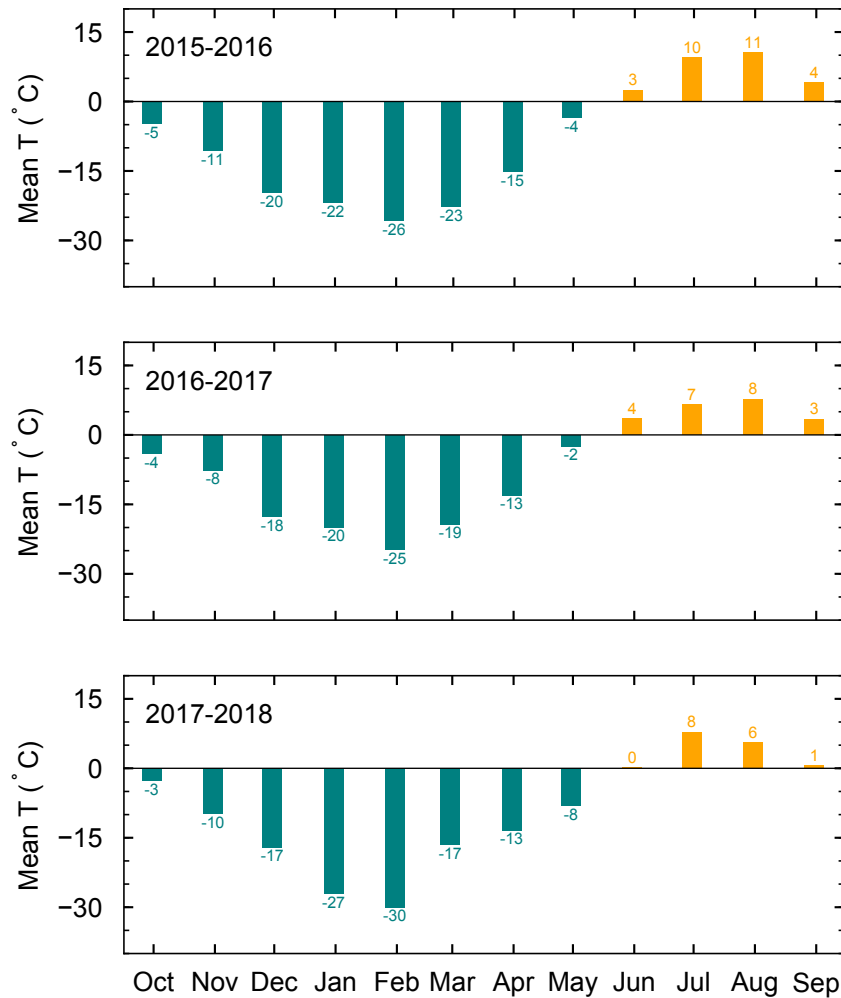


Figure S9: Monthly mean air temperature from 2015 to 2018 measured at Salluit airport.

Freezing and thawing degree-days at Salluit airport

The freezing and thawing degree-days (FDD and TDD) were computed from the Salluit airport data. Their cumulative sum over a period is typically used to characterize how cold or warm that period (Permafrost Subcommittee, 1988). The Ouranos consortium for instance computes the annual cumulative sum of freezing and thawing degree-days for their climate projections and provide them as indicators (Mailhot and Chaumont, 2017).

FDD and TDD are defined in Eq.(1):

$$\text{FDD}(T) = 0 \text{ if } T > 0, |T| \text{ if } T \leq 0 \quad (1a)$$

$$\text{TDD}(T) = T \text{ if } T > 0, 0 \text{ if } T \leq 0 \quad (1b)$$

where T is the daily mean temperature (NSIDC, 2019).

Using the Salluit airport daily temperature time-series, the monthly cumulative freezing and thawing degree-days were computed from 2015 to 2018. These are presented in Fig. S10. Winter was earliest in 2015, where the months of October, November and December were the coldest of the three years. The mildest winter was 2016-2017, with the warmest months of January through April. The coldest winter occurred in 2017-2018, with colder temperatures in January and February than in the two previous years. The latest spring was also in 2018, which featured the coldest months of May and June observed in the study.

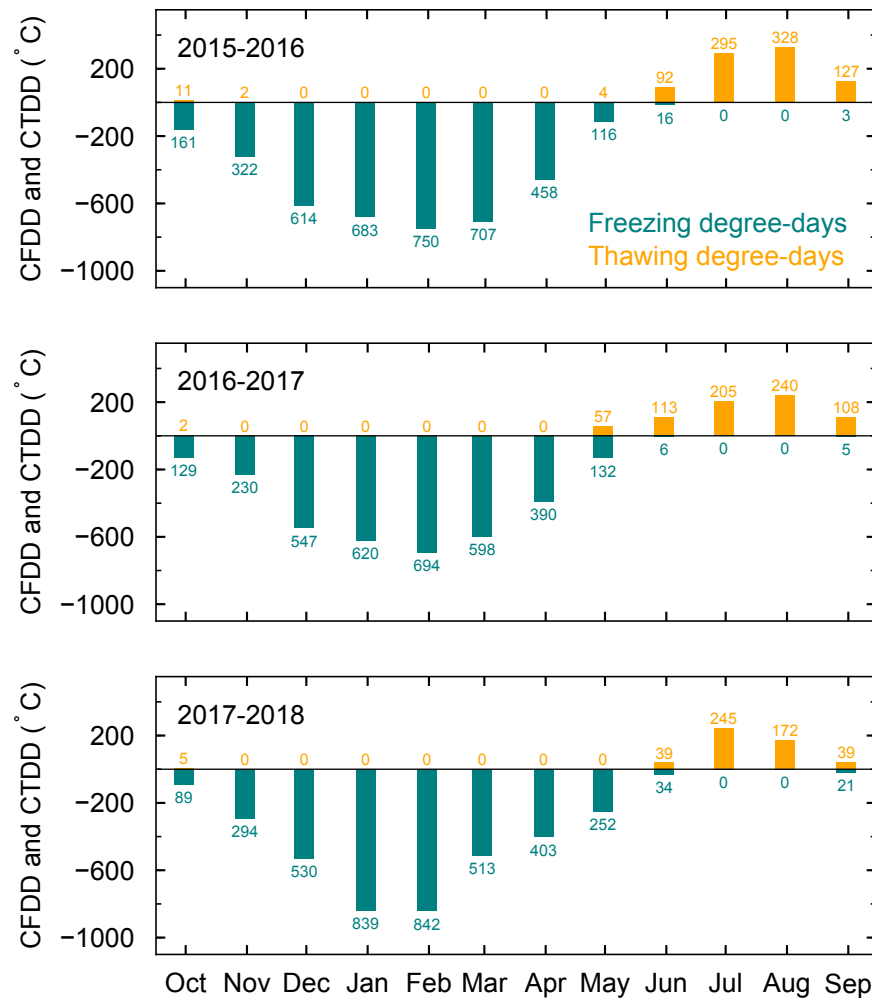


Figure S10: Monthly cumulative freezing (CFDD, in teal) and thawing (CTDD, in orange) degree-days from 2015 to 2018 at Salluit airport.

References

Mailhot, A., and D. Chaumont. 2017. "Élaboration Du Portrait Bioclimatique Futur Du Nunavik - Tome II. Rapport présenté au Ministère de la forêt, de la faune et des parcs." Montréal, Que.: Ouranos.

Permafrost Subcommittee, Associate Committee on Geotechnical Research, National Research Council of Canada, ed. 1988. *Glossary of Permafrost and Related Ground-Ice Terms*. Technical Memorandum 142. Ottawa, Ont.: Associate Committee on Geotechnical Research, National Research Council of Canada.